Geophysical Research Letters

RESEARCH LETTER
10.1029/2021GL097436

# Swift Weathering Response on Floodplains During the Paleocene-Eocene Thermal Maximum

**Evan J. Ramos[1,2], Daniel O. Breecker[1], Jaime D. Barnes[1], Fangliang Li[1,3], Philip D. Gingerich[4], Staci L. Loewy[1], Aaron M. Satkoski[1], Allison A. Baczynski[5], Scott L. Wing[6], Nathaniel R. Miller[1], and John C. Lassiter[1]**

[1]Department of Geologic Sciences, The University of Texas at Austin, Austin, TX, USA, [2]Now at Department of Earth, Environmental & Planetary Sciences, Rice University, Houston, TX, USA, [3]State Key Laboratory of Marine Geology, Tongji University, Shanghai, China, [4]Museum of Paleontology, Research Museum Center, University of Michigan, Ann Arbor, MI, USA, [5]Department of Geosciences, Pennsylvania State University, University Park, PA, USA, [6]Department of Paleobiology, Smithsonian Institution, Washington, DC, USA

**Abstract** Silicate weathering is thought to increase and offset the rapid, massive input of $CO_2$ into the atmosphere and ocean during the Paleocene-Eocene Thermal Maximum (PETM), but few nonmarine records have been used to quantify this. We probe changes in silicate weathering intensity by measuring Li isotope ratios of bedrock and ancient floodplain deposits spanning the PETM in the Bighorn Basin, Wyoming (USA). Our results reveal a rapid increase in silicate weathering intensity during the PETM that remained high during at least the initial stage of climate recovery. Additionally, we determine that soils that formed farthest from ancient river channels underwent larger weathering changes than near-channel soils. Alongside increased temperatures and $pCO_2$, the simplest explanation for this response relates to increased seasonal fluctuations in water table height in the floodplain that promote dissolution and precipitation reactions. These findings newly demonstrate that weathering on floodplains, like mountain hillslopes, responds to climate change.

**Plain Language Summary** The chemical breakdown of silicate minerals on continents promotes the withdrawal of $CO_2$ from the ocean and atmosphere. This process is thought to be enhanced when $CO_2$ rapidly enters the ocean and atmosphere, such as during past climate change events like the Paleocene-Eocene Thermal Maximum (PETM). Although this enhancement of silicate weathering is found in global carbon cycle models and the chemistry of marine rocks, less terrestrial evidence exists for how, where, and to what extent silicate minerals weathered during the PETM. In this study, we measured the chemistry of bedrock and ancient floodplain sediment that span the PETM in the well-studied Bighorn Basin, Wyoming (USA) to quantify changes in silicate weathering intensity. We find that silicate weathering intensity increases rapidly (within 7,000 years of the onset of the PETM) and remains elevated even as climate has begun to return to its pre-perturbed state. We also determine that soils that formed farthest from ancient river channels underwent larger weathering changes than near-channel soils, suggesting active weathering responses on floodplains. Alongside high $CO_2$ contents and warmer temperatures, the simplest explanation for this weathering response relates to soil hydrology, where increased water flow through soils caused by fluctuating water tables enhanced weathering.

**Key Points:**

- A terrestrial silicate weathering response quantified during the Paleocene-Eocene Thermal Maximum (PETM)
- Weathering intensity increases rapidly after PETM, with stronger responses found in floodplain soils farthest from ancient channel
- Weathering response in floodplain linked to hydroclimate and soil hydrology

**Supporting Information:**

Supporting Information may be found in the online version of this article.

**Correspondence to:**

E. J. Ramos,
evan.j.ramos@rice.edu

**Citation:**

Ramos, E. J., Breecker, D. O., Barnes, J. D., Li, F., Gingerich, P. D., Loewy, S. L., et al. (2022). Swift weathering response on floodplains during the Paleocene-Eocene Thermal Maximum. *Geophysical Research Letters*, *49*, e2021GL097436. https://doi.org/10.1029/2021GL097436

Received 15 DEC 2021
Accepted 3 MAR 2022



## 1. Introduction

The Paleocene-Eocene Thermal Maximum (PETM) was a 190 kyr-long event during which an abrupt input of carbon to the ocean and atmosphere increased global average temperatures by 5–8°C (McInerney & Wing, 2011; Wing et al., 2005), more than doubled atmospheric $CO_2$ concentrations (Gutjahr et al., 2017; Haynes & Hönisch, 2020, Figure 1a), and profoundly changed marine and terrestrial biomes (McInerney & Wing, 2011; Wing et al., 2005). Although the conditions that induced and sustained the hyperthermal event have been studied extensively (Bowen et al., 2015; Denis et al., 2021; Gutjahr et al., 2017; Inglis et al., 2021; Lyons et al., 2019), the processes allowing for climatic recovery remain less well understood. Silicate weathering and organic carbon (OC) burial are processes known to promote the withdrawal of carbon from the exosphere (i.e., ocean and atmosphere) and are thus posited to have enabled global climate to return to its pre-PETM state (Bowen & Zachos, 2010; Komar & Zeebe, 2011; Torfstein et al., 2010). Continental erosion rates increased after the onset of the PETM (John et al., 2012; Sharman et al., 2017) which likely enhanced riverine fluxes of OC

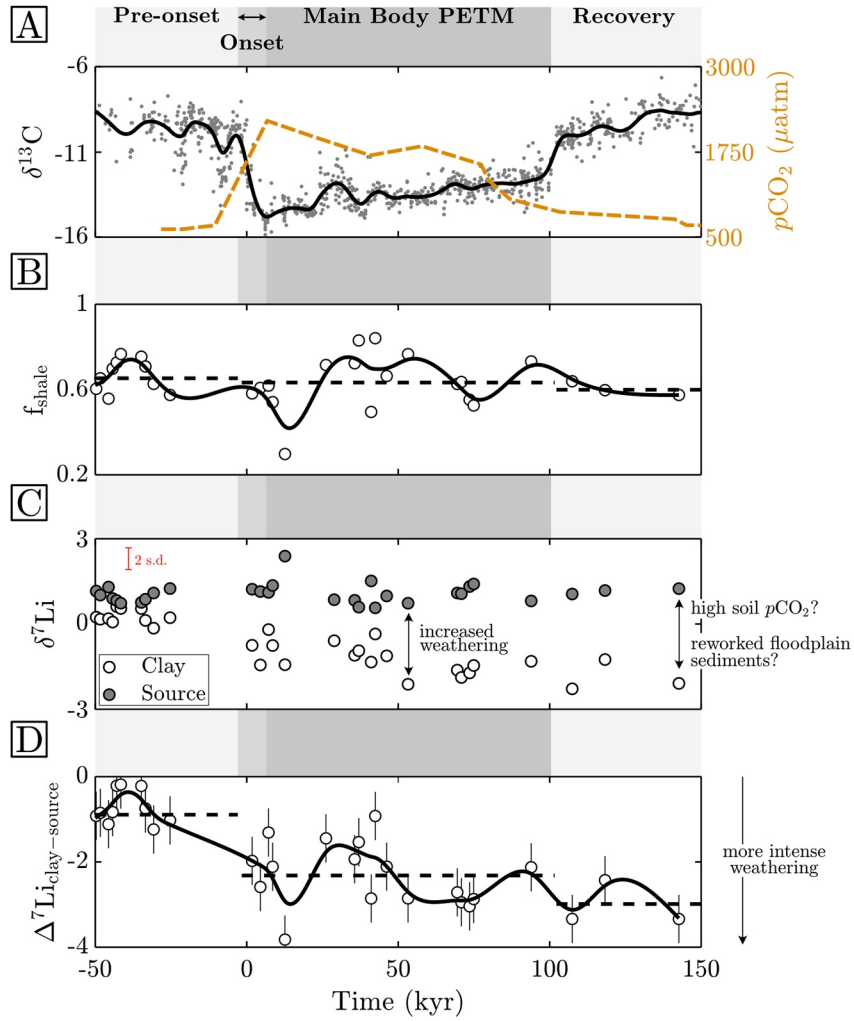


**Figure 1.** Atmospheric and soil chemistry across the Paleocene-Eocene Thermal Maximum. Gray vertical bands represent key time intervals across the event (McInerney & Wing, 2011; Kraus et al., 2015) and time is presented relative to the onset of the carbon isotope excursion. (a) Compilation of pedogenic carbonate $\delta^{13}C$ values from the Bighorn Basin (van der Meulen et al., 2020) and model-derived atmospheric $pCO_2$ partial pressures (Haynes & Hönisch, 2020). The black line corresponds to locally weighted mean carbonate $\delta^{13}C$ values with a 2.5% averaging window. (b) Mixing model-determined fractions of primary shale sediments ($f_{shale}$) from which secondary clays formed. The horizontal black dashed lines are mean values over pre-onset, onset + main body, and recovery time intervals, and the black curve corresponds to locally weighted mean values with a 2.5% averaging window. (c) Measured paleosol clay (<2 μm size fraction) $\delta^7Li$ values and mixing model-determined, weighted average source rock $\delta^7Li$ values for each paleosol. The red error bar corresponds to a maximum, conservative error for each datum (0.5‰, 2 s.d.). (d) $\Delta^7Li_{clay\text{-}source}$ values (i.e., $\delta^7Li_{clay} - \delta^7Li_{source}$) for each paleosol (error is propagated from conservative error for $\delta^7Li_{clay}$ and $\delta^7Li_{source}$ values). The horizontal black dashed lines are mean values over pre-onset, onset + main body, and recovery time intervals, and the black curve corresponds to locally weighted mean values with a 2.5% averaging window.

and dissolved weathering products to the ocean (Hilton & West, 2020). The composition of marine sediments (Dickson et al., 2015; Komar & Zeebe, 2011; Penman et al., 2016; Pogge von Strandmann et al., 2021; Ravizza et al., 2001; Self-Trail et al., 2012) and models of the carbon and silicon cycles (Komar & Zeebe, 2011; Panchuk et al., 2008; Penman, 2016) corroborate these increases, but comparatively less is known about how or where silicate weathering responded on continents. To improve upon these marine records and model findings, more geochemical evidence from nonmarine sedimentary archives needs to be gathered.

Landscapes respond unevenly to climatic perturbations (Romans et al., 2016; Whipple, 2009), yet a key variable that underpins silicate weathering responses across continents is the supply of fresh, un-weathered minerals to near-surface weathering zones. Mountain hillslopes are a dominant locus for silicate weathering in modern

environments (Larsen et al., 2014) because incising rivers generate relief that enhances the supply of fresh bedrock to the Earth's surface. The responsiveness of river incision to climate (Murphy et al., 2016) suggests that silicate weathering in mountain hillslopes may be the primary mechanism by which $CO_2$ is sequestered after hyperthermal events. However, these eroding landscapes are poorly preserved in the geologic record.

In contrast, floodplains are readily preserved in sedimentary records and serve as significant repositories of past Earth surfaces. Yet, the controls of silicate weathering in floodplains are less well understood than in mountain hillslopes. Generally, river-borne sediments, having already undergone weathering in the upper reaches of catchments (Dosseto et al., 2006), are delivered to adjacent floodplains during avulsions and overbank deposition. Low supply of fresh sediments and long fluid-rock interaction time, characteristic of floodplains, favor high silicate weathering intensities (Bouchez et al., 2014; Dellinger et al., 2014, 2017). Globally, however, the resultant silicate weathering flux from floodplains is variable, amounting to as little as 10% of the net catchment weathering flux in some drainages (e.g., Amazon floodplain; Bouchez et al., 2014) to upwards of 70% in others (e.g., Ganges floodplain; Bickle et al., 2018). Moreover, in ancient floodplain deposits, conflicting evidence exists regarding the silicate weathering response to changes in climate across Paleogene hyperthermal events. Despite the similarity in magnitude and direction of change in climate during these global events, some ancient floodplains contain evidence of marked increases in weathering intensity (Clechenko et al., 2007), whereas others show little change (Wang et al., 2017). The disparate responses may be attributed to differences in regional hydroclimate during the body of the event (Carmichael et al., 2018; Rush et al., 2021) or other autogenic controls (e.g., Hajek & Straub, 2017) that modulate water-rock interactions. At a minimum, further efforts to refine controls of silicate weathering in floodplains are necessary to evaluate their role in climate modulation.

In this study, we unravel the silicate weathering response to the PETM in a well-studied, ancient floodplain in the Bighorn Basin, Wyoming, USA. The difference between the Li isotope compositions of river suspended sediments ($\delta^7Li_{suspended}$) and bedrock ($\delta^7Li_{source}$), notated as $\Delta^7Li_{suspended\text{-}source}$, have been shown to relate to silicate weathering intensity (Dellinger et al., 2017); herein, we instead characterize weathering intensities by comparing the isotopic compositions of bedrock units in the basin with the clay-size fraction in paleosols developed in floodplain sediment (i.e., $\Delta^7Li_{clay\text{-}source}$). We document the variability of silicate weathering intensity within a floodplain and underscore the important roles of landscape position and hydroclimate in driving weathering trends.

## 2. Geologic Setting and Samples

All samples were collected in the Bighorn Basin in northern Wyoming, USA: an alluvial, intermontane basin (Dickinson et al., 1988) that formed and filled during the Laramide orogeny, 66–50 Ma (Figure S1 in Supporting Information S1). PETM stratigraphic sections in the Bighorn Basin have been described from multiple outcrops and are typically 20–45 m thick and are composed of well-preserved alluvial channel sandstones and floodplain siltstones and mudstones that have undergone variable degrees of pedogenesis (Baczynski et al., 2017; Bowen et al., 2001, 2015; Koch et al., 1992; Kraus & Riggins, 2007). Before and after the PETM, Bighorn Basin floodplains supported mixed broad-leaved deciduous and evergreen forests composed of angiosperms and conifers whose living relatives are most diverse in humid, subtropical climates; leaf physiognomic proxies also suggest a warm, humid paleoclimate (Peppe et al., 2011; Wing & Greenwood, 1993; Wing & Currano, 2013; Wing et al., 1995). In contrast, fossil plants from the body of the negative carbon isotope excursion (CIE) associated with the PETM have living relatives that are most diverse in tropical dry climates; leaf physiognomic analyses, paleosol features, basin stratigraphy, and climate models support an increase of ~5°C in mean annual temperature (MAT), a decrease in water availability (Currano et al., 2008; Kraus et al., 2013; Peppe et al., 2011; Wing & Currano, 2013; Wing et al., 2005), and enhanced seasonality of precipitation (Carmichael et al., 2018; Foreman, 2014; Kraus et al., 2015; Rush et al., 2021; Shellito et al., 2003). Fossil plants from the recovery phase of the CIE indicate a return to a cooler, wetter climate (Wing & Currano, 2013).

For this study, paleosols were sampled at Polecat Bench in Powell, WY, which is a well-characterized outcrop positioned near the basin axis in the northern part of the basin (Kraus et al., 2015 and references therein; see Section S1 in Supporting Information S1 for expanded description of the site). Stratigraphic elevations were converted to time with respect to the CIE using a newly refined, high-resolution age model (van der Meulen et al., 2020). In accordance with sedimentological features, all paleosols were classified as either composite, crevasse splay, or cumulative soils (Kraus, 1999), which are facies characterizations of paleosols that describe

soil formation in response to episodic (composite, crevasse splay) or quasi-continuous (cumulative) sedimentation. These soil facies qualitatively indicate the paleo-landscape position of the soil in the floodplain at the time of formation (i.e., composite and crevasse splay are channel proximal whereas cumulative is more distal). Bedrock samples, which are thought of as potential source rocks for Paleogene floodplain deposits and include Precambrian basement through Cretaceous shales (Baczynski et al., 2016), were retrieved from outcrops on the flanks of the basin (Figure S1 in Supporting Information S1; Table S1).

## 3. Deducing Paleogene Silicate Weathering Intensity

The clay-sized fraction (<2 μm) of paleosols and whole rock powders of possible source rocks were analyzed for major and trace element concentrations and Li isotope ratios. Because $^6$Li is preferentially incorporated into authigenic clays during weathering, the comparison of $\delta^7$Li values of sediment with the $\delta^7$Li values of their source indicates the intensity of weathering (Dellinger et al., 2017). Floodplains typically contain sediment from multiple types of bedrock, making such comparisons difficult. We measure immobile element concentrations to overcome this complexity. The abundances of these elements, such as Ti, Zr, Al, and Cs (Bouchez et al., 2011; Dellinger et al., 2017), and their ratios to one another do not change during weathering, allowing us to determine the provenance of clays (detrital and authigenic) in floodplain paleosols. Critically, authigenic clays that form from the chemical weathering of primary silicate sediment will have an immobile element composition that reflects a mixture of parent materials (see Supporting Information S1 for detailed explanation of methods). Using an immobile element mixing model, two primary endmembers were identified: a Cretaceous shale unit (Cody Fm.) and feldspar-bearing igneous rock characteristic of regional basement (Figure S5 in Supporting Information S1). Here we are interested in the "reweathering" of the shale that occurred during the Paleogene and therefore, although the shale contains weathering products that formed during the Cretaceous, we treat the shale as a source and compare paleosol clays to it. We express proportions of the shale and igneous rock endmembers in the paleosols as

$$f_{\text{shale}} + f_{\text{igneous}} = 1 \quad (1)$$

where $f_{\text{shale}}$ and $f_{\text{igneous}}$ correspond to the fractions of shale and igneous rocks, respectively. These fractions, along with measured endmember $\delta^7$Li values and Li concentrations, were used to compute weighted average $\delta^7\text{Li}_{\text{source}}$ values for each paleosol (descriptions of analytical and computational methods can be found in Supporting Information S1). With this, we compute $\Delta^7\text{Li}_{\text{clay-source}}$ values as an indicator of weathering intensity, where more negative $\Delta^7\text{Li}_{\text{clay-source}}$ values indicate more intense weathering (Dellinger et al., 2017).

The measured $\delta^7\text{Li}_{\text{clay}}$ values range from −2.3 to +0.6‰. Potential parent materials span a much wider range of $\delta^7$Li values (−4.1 to +25.1‰; Li/Al-weighted average value of 0.8 ± 1.3‰ (1 s.d., $n = 12$); see Table S1). Given our determination of endmembers, we find $\delta^7\text{Li}_{\text{shale}} = +0.3$‰ (measured $\delta^7$Li value of Cody Fm. sample) and $\delta^7\text{Li}_{\text{igneous}} = +5.1$‰ (average $\delta^7$Li value of two igneous rock samples), effectively narrowing the range of potential $\delta^7\text{Li}_{\text{source}}$ values. With these values, $\delta^7\text{Li}_{\text{source}}$ values are computed and their range is from +1.1 to +2.4‰ (see Supporting Information S1 for $\delta^7\text{Li}_{\text{source}}$ calculation methods; Table S1). Because all $\delta^7\text{Li}_{\text{clay}}$ values are smaller than the endmember $\delta^7$Li values, clay-sized fractions are likely composed of primarily authigenic clays. Importantly, in contrast to the $\delta^7\text{Li}_{\text{source}}$ values that are roughly constant across the PETM due to relatively steady $f_{shale}$ (Figure 1b), $\delta^7\text{Li}_{\text{clay}}$ values steadily decrease through the main body and into the recovery phase of the event (Figure 1c). We therefore infer that weathering intensities increase during the main body of the event and remain high into the recovery phase (Figure 1d).

When samples are grouped in accordance with their soil facies (composite, crevasse splay, or cumulative soils; see Figure S2 in Supporting Information S1), $\Delta^7\text{Li}_{\text{clay-source}}$ values show consistent direct correlations with the fraction of primary shale ($f_{shale}$) (Figure 2; Figure S5 in Supporting Information S1), where higher $f_{shale}$ correlates with lower weathering intensities. If we detrend each sample grouping (Figure 2) to account for variations in $f_{shale}$ (see Section S4 in Supporting Information S1) and consider the average change in weathering intensities among a soil facies during the PETM, we determine that crevasse splay soils undergo an average $\Delta^7\text{Li}_{\text{clay-source}}$ excursion of −1.3‰ whereas cumulative soils undergo a −2.2‰ excursion (Figure 3).

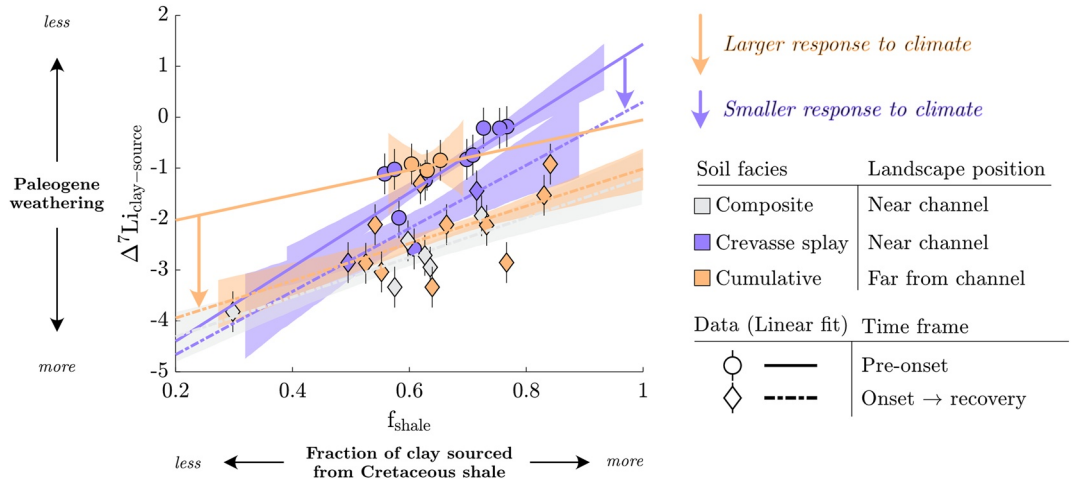


**Figure 2.** $\Delta^7Li_{clay\text{-}source}$ values as a function of $f_{shale}$ (error bars are 2 s.d.). Data are grouped according to soil facies and time intervals of the Paleocene-Eocene Thermal Maximum, and lines correspond to linear fits through corresponding data groups. There is a consistent relationship between $\Delta^7Li_{clay\text{-}source}$ values and $f_{shale}$.

## 4. Influence of Climate and Landscape Position on Floodplain Weathering

The Li isotope data indicate a rapid and substantial increase in silicate weathering intensity in response to the climatic perturbation. This stepwise increase in weathering intensity during the PETM coincides with major shifts in atmospheric $pCO_2$ (Gutjahr et al., 2017; Haynes & Hönisch, 2020), hydroclimate (Kraus et al., 2013, 2015), floral composition (Wing & Currano, 2013; Wing et al., 2005), and floodplain architecture (Abdul Aziz et al., 2008; Foreman, 2014) in the Bighorn Basin. The >3‰ negative excursion in $\delta^7Li_{clay}$ values in this study is likely driven by changes in weathering resulting from these environmental changes because long-term sediment aggradation rates (van der Meulen et al., 2020), provenance (May et al., 2013), and $\delta^7Li_{source}$ values remained constant across the PETM (Figure 1b; see Section S1 in Supporting Information S1). Notably, the magnitude of this excursion agrees with others from marine shale and carbonate transects that span the PETM (Pogge von Strandmann et al., 2021).

Several lines of evidence suggest that a combination of environmental variables is necessary to explain these weathering trends. First, a simple control by temperature/$pCO_2$ on observed trends can be ruled out because silicate weathering intensity (a) fluctuates during the main body of the PETM when temperature/$pCO_2$ are relatively steady and (b) remains high in the recovery phase as temperature/$pCO_2$ have returned to pre-PETM levels. Second, neither variations in the lithologic composition of soils (i.e., $f_{shale}$) nor changes in soil facies across the PETM can fully explain the secular trend in weathering intensity; stepwise decreases in $\Delta^7Li_{clay\text{-}source}$ values during the PETM remain after each sample is detrended to average $f_{shale}$ (Figure S7 in Supporting Information S1) and decreases in average $\Delta^7Li_{clay\text{-}source}$ values are found among each soil facies (Figure 3). Instead, distinct weathering relationships are best discerned when $f_{shale}$, climate, and soil facies are considered together (Figure 2). Shales, which are lithified byproducts of past continental weathering, weather less readily at Earth's surface than primary igneous rock-derived minerals like plagioclase or biotite (White & Buss, 2014), explaining the consistent inverse relationships between weathering intensity and $f_{shale}$. This lithologic control is then modulated by climate and landscape position. Higher temperatures and $pCO_2$ enable more intense silicate weathering (Winnick & Maher, 2018) whether the samples have high or low values of $f_{shale}$ (Figure 2). Importantly, the difference in weathering trends between varying climate states is most pronounced in soils that formed far from the channel (Figure 3). Composite and crevasse splay soils, which are coarser grained, better drained, and

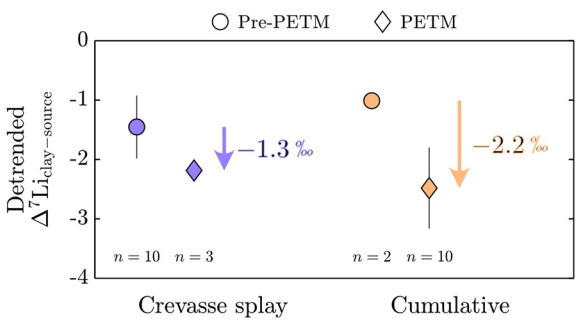


**Figure 3.** $f_{shale}$-detrended $\Delta^7Li_{clay\text{-}source}$ values of crevasse splay and cumulative soils. Each soil $\Delta^7Li_{clay\text{-}source}$ value was detrended to account for lithologic differences (see Section S4 in Supporting Information S1 for detrending method description and rationale). Mean detrended $\Delta^7Li_{clay\text{-}source}$ values and their standard deviations are presented for each data group; the number of samples in each group is listed beneath the means; the magnitude of the Li isotope excursion between pre-Paleocene-Eocene Thermal Maximum (pre-PETM) and PETM paleosols is listed to the right each soil facies.

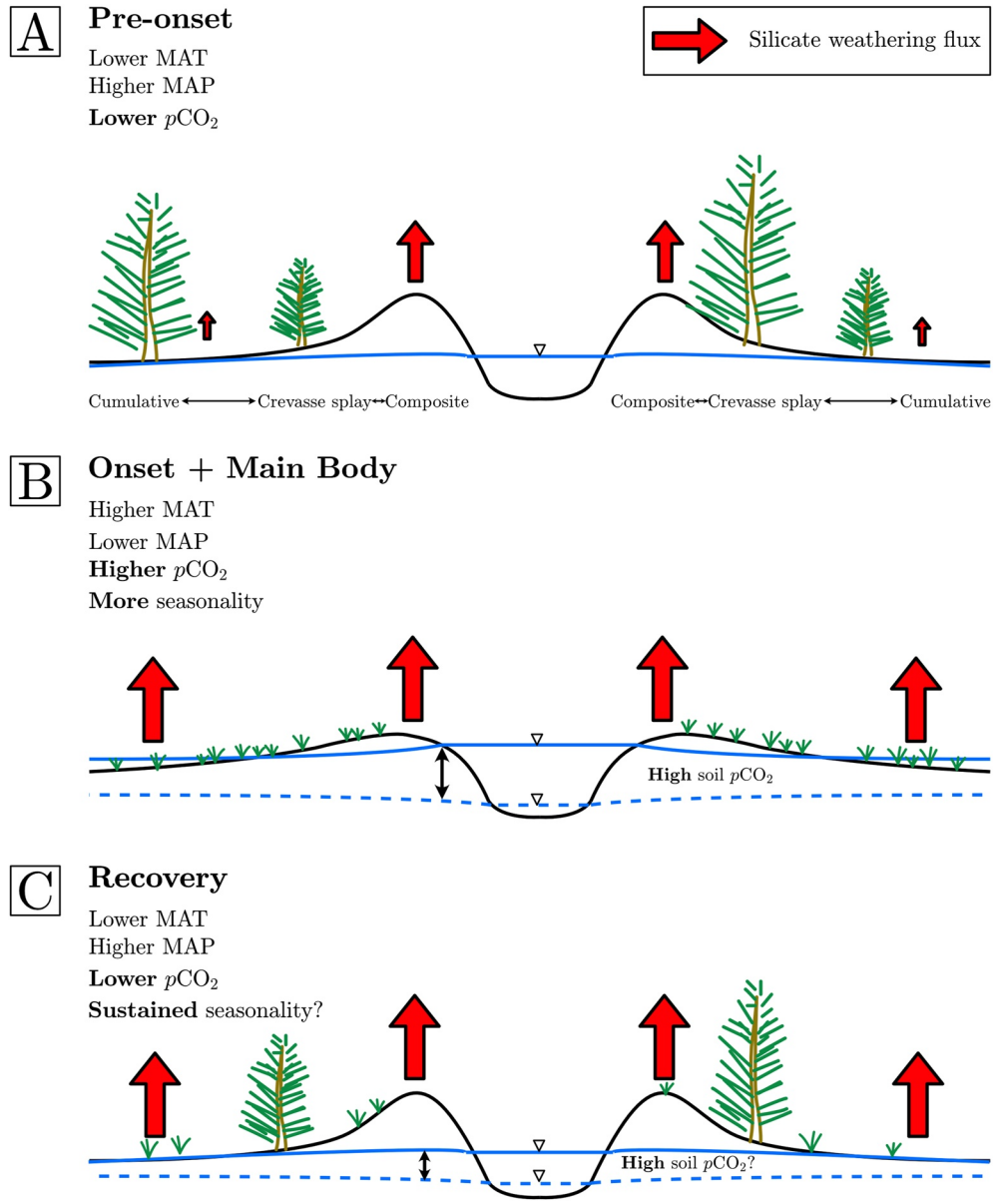


**Figure 4.** Conceptual cross-sections of floodplains in the Bighorn Basin spanning the pre-onset (a), onset and main body (b), and recovery (c) phases of the Paleocene-Eocene Thermal Maximum. The relative location of each soil facies (composite, crevasse splay, and cumulative) is listed beneath cross-section in panel A but applies to each cross-section. Blue lines correspond to the elevation(s) of the water table (fluctuating in panels B and C). Red arrows indicate locations of silicate weathering fluxes in the floodplain and the sizes are their relative magnitudes (larger = greater).

topographically high within floodplains (Kraus, 1999), form in oxidizing conditions that more readily facilitate silicate weathering reactions. Cumulative soils, in contrast, tend to be finer grained and more poorly drained, favoring reducing conditions and slow water movement that keep silicate minerals from chemically weathering. Therefore, in this alluvial system, when the floodplain soils become better drained during the body of the hyperthermal event, more limitations of silicate weathering are removed in cumulative soils than their near-channel counterparts, yielding a stronger silicate weathering response despite reduced availability of water (Wing & Currano, 2013).

The simplest explanation for these weathering trends is the fluctuation of the water table in response to increased seasonality during the PETM (Figure 4). In addition to increases in MAT and $pCO_2$ during the main body, mean annual precipitation (MAP) in the Bighorn Basin decreased and became more seasonal. Large rainfall events and

increased evapotranspiration in the basin led to better-drained soils and large fluctuations in water table height (Kraus et al., 2013). As a result, soil water contents would likely change widely throughout a year, perturbing the saturation state of the aqueous solutions in soil and thereby catalyzing mineral dissolution and precipitation reactions (e.g., Golla et al., 2021). In contrast to well-drained proximal soils, distal soils retain water due to their high clay content (i.e., due to high matric potentials) and therefore require greater changes in hydroclimate and water table height to enable oxidative weathering. Periods of poor soil drainage and high MAP, or even low MAP and limited water availability, during the body of the PETM may also explain the occurrences of low silicate weathering intensity. We postulate that the two likeliest causes of relatively high silicate weathering intensity during the recovery phase were either (a) sustained seasonality of rainfall (Kraus et al., 2015) and a return to wetter conditions (Wing & Currano, 2013) that promote intense weathering or (b) persistent weathering below the water table (Golla et al., 2021) as MAP increased, water tables steadily rose, and weathering environments transitioned to a new equilibrium state. Although in need of further evidence, a third possibility was that with the return of conifer to the vegetation increased soil root mass that sustained high soil $pCO_2$ and transiently increased weathering rates (Algeo & Scheckler, 2010) despite atmospheric $pCO_2$ returning to pre-PETM levels. A fourth possibility is that detrital floodplain clays or upstream hillslope clays (i.e., those with low $\delta^7Li$ values) compose a significant proportion of paleosol clay-sized fractions that mask an undetected decrease in silicate weathering intensity during the recovery phase. Evidence of floodplain reworking (e.g., clay rip-up clasts in sandstone deposits, crevasse splay deposits), a process that would remobilize sediments and lead to their deposition downstream, is found throughout this stratigraphic section (Kraus et al., 2015). Yet, if this reworking pervasively influenced weathering trends, one would expect a lagged $\Delta^7Li_{clay\text{-}source}$ excursion at the onset of the event (Figure 1d). The lack of any substantial lag at the onset of the PETM, along with the consistency of weathering trends among soil facies and their agreement with principles of floodplain hydrology, suggests that the detrital component in the clay-sized fraction is minimal. Ultimately, persistently low $\Delta^7Li_{clay\text{-}source}$ values in the recovery phase, which are not seen in marine shale sections (Pogge von Strandmann et al., 2021), may indicate that while continental-scale weathering intensity returned to pre-PETM lows, local conditions within the Bighorn Basin favored a more sluggish return to low weathering intensities.

Altogether, these findings demonstrate that floodplain weathering dynamically responds to climate change and further illustrate the utility of Li isotope ratios in detecting weathering changes in sedimentary archives (Pogge von Strandmann et al., 2021). Unlike weathering on mountain hillslopes, the climatic sensitivity of which is tied to the kinetics of silicate mineral dissolution (Bufe et al., 2021), floodplain weathering involves mineral residence times long enough to counter these dissolution kinetics (Dosseto et al., 2006; Torres et al., 2017). Instead, we conclude that weathering on floodplains is sensitive to climatically driven changes in water flow through soils where better soil drainage begets more intense weathering. The rapid and large weathering response to climate change in the Bighorn Basin during the PETM might be characteristic of intermontane basins whose steady supply of fresh silicate sediment from adjacent uplifts (van der Meulen et al., 2020) enable strong silicate weathering responses. These findings ultimately expand upon recent studies that argue for floodplains as carbon sinks (Bufe et al., 2021; Torres et al., 2016) and newly underscore the relevance of floodplain biogeochemical cycling in the carbon cycle over much wider timescales than previously thought.

**Acknowledgments**
The authors extend many thanks to Mark Torres, Hima Hassenruck-Gudipati, David Mohrig, Josh West, Brady Foreman, and Liz Hajek for stimulating discussions and scientific input during this project; to Kate Andrzejewski and Neil Tabor for graciously sharing facilities and assisting with clay centrifugation, which was undertaken at Southern Methodist University; Sarah George, Simon Scarpetta, and Laura Arnold for assistance with field work in Summer 2019; two anonymous reviewers whose input improved the original manuscript; and Harihar Rajaram for careful editorial handling. Laboratory and field work was funded through grants from the Geological Society of America and the Jackson School of Geosciences to the first author.

## Data Availability Statement

Supporting Information files Table S1 and S2 contain all gathered data and MATLAB codes used to generate plots and mixing models calculations are available through Zenodo, which can be accessed through https://doi.org/10.5281/zenodo.6342274.

## References

Abdul Aziz, H., Hilgen, F. J., van Luijk, G. M., Sluijs, A., Kraus, M. J., Pares, J. M., & Gingerich, P. D. (2008). Astronomical climate control on paleosol stacking patterns in the upper Paleocene–lower Eocene Willwood Formation, Bighorn Basin, Wyoming. *Geology*, *36*(7), 531–534. https://doi.org/10.1130/g24734a.1

Algeo, T. J., & Scheckler, S. E. (2010). Land plant evolution and weathering rate changes in the Devonian. *Journal of Earth Sciences*, *21*(1), 75–78. https://doi.org/10.1007/s12583-010-0173-2

Baczynski, A. A., McInerney, F. A., Wing, S. L., Kraus, M. J., Bloch, J. I., & Secord, R. (2017). Constraining paleohydrologic change during the Paleocene-Eocene Thermal Maximum in the continental interior of North America. *Palaeogeography, Palaeoclimatology, Palaeoecology*, *465*, 237–246. https://doi.org/10.1016/j.palaeo.2016.10.030

Baczynski, A. A., McInerney, F. A., Wing, S. L., Kraus, M. J., Morse, P. E., Bloch, J. I., et al. (2016). Distortion of carbon isotope excursion in bulk soil organic matter during the Paleocene-Eocene Thermal Maximum. *Bulletin*, *128*(9–10), 1352–1366. https://doi.org/10.1130/b31389.1

Bickle, M. J., Chapman, H. J., Tipper, E., Galy, A., Christina, L., & Ahmad, T. (2018). Chemical weathering outputs from the flood plain of the Ganga. *Geochimica et Cosmochimica Acta*, *225*, 146–175. https://doi.org/10.1016/j.gca.2018.01.003

Bouchez, J., Gaillardet, J., France-Lanord, C., Maurice, L., & Dutra-Maia, P. (2011). Grain size control of river suspended sediment geochemistry: Clues from Amazon River depth profiles. *Geochemistry, Geophysics, Geosystems*, *12*(3). https://doi.org/10.1029/2010gc003380

Bouchez, J., Gaillardet, J., & von Blanckenburg, F. (2014). Weathering intensity in lowland river basins: From the Andes to the Amazon mouth. *Procedia Earth and Planetary Science*, *10*, 280–286. https://doi.org/10.1016/j.proeps.2014.08.063

Bowen, G. J., Koch, P. L., Gingerich, P. D., Norris, R. D., Bains, S., & Corfield, R. M. (2001). Refined isotope stratigraphy across the continental Paleocene-Eocene boundary on Polecat Bench in the northern Bighorn Basin. *Paleocene-Eocene Stratigraphy and Biotic Change in the Bighorn and Clarks Fork Basins, Wyoming. University of Michigan Papers on Paleontology*, *33*, 73–88.

Bowen, G. J., Maibauer, B. J., Kraus, M. J., Röhl, U., Westerhold, T., Steimke, A., et al. (2015). Two massive, rapid releases of carbon during the onset of the Palaeocene–Eocene thermal maximum. *Nature Geoscience*, *8*(1), 44–47. https://doi.org/10.1038/ngeo2316

Bowen, G. J., & Zachos, J. C. (2010). Rapid carbon sequestration at the termination of the Palaeocene–Eocene Thermal Maximum. *Nature Geoscience*, *3*(12), 866–869. https://doi.org/10.1038/ngeo1014

Bufe, A., Hovius, N., Emberson, R., Rugenstein, J. K., Galy, A., Hassenruck-Gudipati, H. J., & Chang, J. M. (2021). Co-variation of silicate, carbonate and sulfide weathering drives $CO_2$ release with erosion. *Nature Geoscience*, *14*(4), 211–216. https://doi.org/10.1038/s41561-021-00714-3

Carmichael, M. J., Pancost, R. D., & Lunt, D. J. (2018). Changes in the occurrence of extreme precipitation events at the Paleocene–Eocene thermal maximum. *Earth and Planetary Science Letters*, *501*, 24–36. https://doi.org/10.1016/j.epsl.2018.08.005

Clechenko, E. R., Kelly, D. C., Harrington, G. J., & Stiles, C. A. (2007). Terrestrial records of a regional weathering profile at the Paleocene-Eocene boundary in the Williston Basin of North Dakota. *The Geological Society of America Bulletin*, *119*(3–4), 428–442. https://doi.org/10.1130/b26010.1

Currano, E. D., Wilf, P., Wing, S. L., Labandeira, C. C., Lovelock, E. C., & Royer, D. L. (2008). Sharply increased insect herbivory during the Paleocene–Eocene Thermal Maximum. *Proceedings of the National Academy of Sciences*, *105*(6), 1960–1964. https://doi.org/10.1073/pnas.0708646105

Dellinger, M., Bouchez, J., Gaillardet, J., Faure, L., & Moureau, J. (2017). Tracing weathering regimes using the lithium isotope composition of detrital sediments. *Geology*, *45*(5), 411–414. https://doi.org/10.1130/g38671.1

Dellinger, M., Gaillardet, J., Bouchez, J., Calmels, D., Galy, V., Hilton, R. G., et al. (2014). Lithium isotopes in large rivers reveal the cannibalistic nature of modern continental weathering and erosion. *Earth and Planetary Science Letters*, *401*, 359–372. https://doi.org/10.1016/j.epsl.2014.05.061

Denis, E. H., Maibauer, B. J., Bowen, G. J., Jardine, P. E., Harrington, G. J., Baczynski, A. A., et al. (2021). Decreased soil carbon in a warming world: Degraded pyrogenic carbon during the Paleocene-Eocene Thermal Maximum, Bighorn Basin, Wyoming. *Earth and Planetary Science Letters*, *566*, 116970. https://doi.org/10.1016/j.epsl.2021.116970

Dickinson, W. R., Klute, M. A., Hayes, M. J., Janecke, S. U., Lundin, E. R., McKittrick, M. A., & Olivares, M. D. (1988). Paleogeographic and paleotectonic setting of Laramide sedimentary basins in the central Rocky Mountain region. *The Geological Society of America Bulletin*, *100*(7), 1023–1039. https://doi.org/10.1130/0016-7606(1988)100<1023:papsol>2.3.co;2

Dickson, A. J., Cohen, A. S., Coe, A. L., Davies, M., Shcherbinina, E. A., & Gavrilov, Y. O. (2015). Evidence for weathering and volcanism during the PETM from Arctic Ocean and Peri-Tethys osmium isotope records. *Palaeogeography, Palaeoclimatology, Palaeoecology*, *438*, 300–307. https://doi.org/10.1016/j.palaeo.2015.08.019

Dosseto, A., Bourdon, B., Gaillardet, J., Maurice-Bourgoin, L., & Allegre, C. J. (2006). Weathering and transport of sediments in the Bolivian Andes: Time constraints from uranium-series isotopes. *Earth and Planetary Science Letters*, *248*(3–4), 759–771. https://doi.org/10.1016/j.epsl.2006.06.027

Foreman, B. Z. (2014). Climate-driven generation of a fluvial sheet sand body at the Paleocene–Eocene boundary in north-west Wyoming (USA). *Basin Research*, *26*(2), 225–241. https://doi.org/10.1111/bre.12027

Golla, J. K., Kuessner, M. L., Henehan, M. J., Bouchez, J., Rempe, D. M., & Druhan, J. L. (2021). The evolution of lithium isotope signatures in fluids draining actively weathering hillslopes. *Earth and Planetary Science Letters*, *567*, 116988. https://doi.org/10.1016/j.epsl.2021.116988

Gutjahr, M., Ridgwell, A., Sexton, P. F., Anagnostou, E., Pearson, P. N., Pälike, H., et al. (2017). Very large release of mostly volcanic carbon during the Palaeocene–Eocene Thermal Maximum. *Nature*, *548*(7669), 573–577. https://doi.org/10.1038/nature23646

Hajek, E. A., & Straub, K. M. (2017). Autogenic sedimentation in clastic stratigraphy. *Annual Review of Earth and Planetary Sciences*, *45*(1), 681–709. https://doi.org/10.1146/annurev-earth-063016-015935

Haynes, L. L., & Hönisch, B. (2020). The seawater carbon inventory at the Paleocene–Eocene Thermal Maximum. *Proceedings of the National Academy of Sciences*, *117*(39), 24088–24095. https://doi.org/10.1073/pnas.2003197117

Hilton, R. G., & West, A. J. (2020). Mountains, erosion and the carbon cycle. *Nature Reviews Earth & Environment*, *1*(6), 284–299. https://doi.org/10.1038/s43017-020-0058-6

Inglis, G. N., Rohrssen, M., Kennedy, E. M., Crouch, E. M., Raine, J. I., Strogen, D. P., et al. (2021). Terrestrial methane cycle perturbations during the onset of the Paleocene-Eocene Thermal Maximum. *Geology*, *49*(5), 520–524. https://doi.org/10.1130/g48110.1

John, C. M., Banerjee, N. R., Longstaffe, F. J., Sica, C., Law, K. R., & Zachos, J. C. (2012). Clay assemblage and oxygen isotopic constraints on the weathering response to the Paleocene-Eocene Thermal Maximum, east coast of North America. *Geology*, *40*(7), 591–594. https://doi.org/10.1130/g32785.1

Koch, P. L., Zachos, J. C., & Gingerich, P. D. (1992). Correlation between isotope records in marine and continental carbon reservoirs near the Palaeocene/Eocene boundary. *Nature*, *358*(6384), 319–322. https://doi.org/10.1038/358319a0

Komar, N., & Zeebe, R. E. (2011). Oceanic calcium changes from enhanced weathering during the Paleocene-Eocene thermal maximum: No effect on calcium-based proxies. *Paleoceanography*, *26*(3). https://doi.org/10.1029/2010pa001979

Kraus, M. J. (1999). Paleosols in clastic sedimentary rocks: Their geologic applications. *Earth-Science Reviews*, *47*(1–2), 41–70. https://doi.org/10.1016/s0012-8252(99)00026-4

Kraus, M. J., McInerney, F. A., Wing, S. L., Secord, R., Baczynski, A. A., & Bloch, J. I. (2013). Paleohydrologic response to continental warming during the Paleocene–Eocene thermal maximum, Bighorn Basin, Wyoming. *Palaeogeography, Palaeoclimatology, Palaeoecology*, *370*, 196–208. https://doi.org/10.1016/j.palaeo.2012.12.008

Kraus, M. J., & Riggins, S. (2007). Transient drying during the Paleocene–Eocene Thermal Maximum (PETM): Analysis of paleosols in the Bighorn Basin, Wyoming. *Palaeogeography, Palaeoclimatology, Palaeoecology*, *245*(3–4), 444–461. https://doi.org/10.1016/j.palaeo.2006.09.011

Kraus, M. J., Woody, D. T., Smith, J. J., & Dukic, V. (2015). Alluvial response to the Paleocene–Eocene thermal maximum climatic event, polecat bench, Wyoming (USA). *Palaeogeography, Palaeoclimatology, Palaeoecology*, *435*, 177–192. https://doi.org/10.1016/j.palaeo.2015.06.021

Larsen, I. J., Montgomery, D. R., & Greenberg, H. M. (2014). The contribution of mountains to global denudation. *Geology*, *42*(6), 527–530. https://doi.org/10.1130/g35136.1

Lyons, S. L., Baczynski, A. A., Babila, T. L., Bralower, T. J., Hajek, E. A., Kump, L. R., et al. (2019). Palaeocene–Eocene thermal maximum prolonged by fossil carbon oxidation. *Nature Geoscience*, *12*(1), 54–60. https://doi.org/10.1038/s41561-018-0277-3

May, S. R., Gray, G. G., Summa, L. L., Stewart, N. R., Gehrels, G. E., & Pecha, M. E. (2013). Detrital zircon geochronology from the Bighorn Basin, Wyoming, USA: Implications for tectonostratigraphic evolution and paleogeography. *The Geological Society of America Bulletin*, *125*(9–10), 1403–1422. https://doi.org/10.1130/b30824.1

McInerney, F. A., & Wing, S. L. (2011). The Paleocene-Eocene Thermal Maximum: A perturbation of carbon cycle, climate, and biosphere with implications for the future. *Annual Review of Earth and Planetary Sciences*, *39*(1), 489–516. https://doi.org/10.1146/annurev-earth-040610-133431

Murphy, B. P., Johnson, J. P., Gasparini, N. M., & Sklar, L. S. (2016). Chemical weathering as a mechanism for the climatic control of bedrock river incision. *Nature*, *532*(7598), 223–227. https://doi.org/10.1038/nature17449

Panchuk, K., Ridgwell, A., & Kump, L. R. (2008). Sedimentary response to Paleocene-Eocene Thermal Maximum carbon release: A model-data comparison. *Geology*, *36*(4), 315–318. https://doi.org/10.1130/g24474a.1

Penman, D. E. (2016). Silicate weathering and North Atlantic silica burial during the Paleocene-Eocene Thermal Maximum. *Geology*, *44*(9), 731–734. https://doi.org/10.1130/g37704.1

Penman, D. E., Turner, S. K., Sexton, P. F., Norris, R. D., Dickson, A. J., Boulila, S., et al. (2016). An abyssal carbonate compensation depth overshoot in the aftermath of the Palaeocene–Eocene Thermal Maximum. *Nature Geoscience*, *9*(8), 575–580. https://doi.org/10.1038/ngeo2757

Peppe, D. J., Royer, D. L., Cariglino, B., Oliver, S. Y., Newman, S., Leight, E., et al. (2011). Sensitivity of leaf size and shape to climate: Global patterns and paleoclimatic applications. *New Phytologist*, *190*(3), 724–739. https://doi.org/10.1111/j.1469-8137.2010.03615.x

Pogge von Strandmann, P. A. E., Jones, M. T., West, A. J., Murphy, M. J., Stokke, E. W., Tarbuck, G., et al. (2021). Lithium isotope evidence for enhanced weathering and erosion during the Paleocene-Eocene Thermal Maximum. *Science Advances*, *7*(42), eabh4224. https://doi.org/10.1126/sciadv.abh4224

Ravizza, G., Norris, R. N., Blusztajn, J., & Aubry, M. P. (2001). An osmium isotope excursion associated with the late Paleocene thermal maximum: Evidence of intensified chemical weathering. *Paleoceanography*, *16*(2), 155–163. https://doi.org/10.1029/2000pa000541

Romans, B. W., Castelltort, S., Covault, J. A., Fildani, A., & Walsh, J. P. (2016). Environmental signal propagation in sedimentary systems across timescales. *Earth-Science Reviews*, *153*, 7–29. https://doi.org/10.1016/j.earscirev.2015.07.012

Rush, W. D., Kiehl, J. T., Shields, C. A., & Zachos, J. C. (2021). Increased frequency of extreme precipitation events in the North Atlantic during the PETM: Observations and theory. *Palaeogeography, Palaeoclimatology, Palaeoecology*, *568*, 110289. https://doi.org/10.1016/j.palaeo.2021.110289

Self-Trail, J. M., Powars, D. S., Watkins, D. K., & Wandless, G. A. (2012). Calcareous nannofossil assemblage changes across the Paleocene–Eocene Thermal Maximum: Evidence from a shelf setting. *Marine Micropaleontology*, *92*, 61–80. https://doi.org/10.1016/j.marmicro.2012.05.003

Sharman, G. R., Covault, J. A., Stockli, D. F., Wroblewski, A. F. J., & Bush, M. A. (2017). Early Cenozoic drainage reorganization of the United States Western Interior–Gulf of Mexico sediment routing system. *Geology*, *45*(2), 187–190. https://doi.org/10.1130/g38765.1

Shellito, C. J., Sloan, L. C., & Huber, M. (2003). Climate model sensitivity to atmospheric $CO_2$ levels in the Early–Middle Paleogene. *Palaeogeography, Palaeoclimatology, Palaeoecology*, *193*(1), 113–123. https://doi.org/10.1016/s0031-0182(02)00718-6

Torfstein, A., Winckler, G., & Tripati, A. (2010). Productivity feedback did not terminate the Paleocene-Eocene Thermal Maximum (PETM). *Climate of the Past*, *6*(2), 265–272. https://doi.org/10.5194/cp-6-265-2010

Torres, M. A., Limaye, A. B., Ganti, V., Lamb, M. P., West, A. J., & Fischer, W. W. (2017). Model predictions of long-lived storage of organic carbon in river deposits. *Earth Surface Dynamics*, *5*(4), 711–730. https://doi.org/10.5194/esurf-5-711-2017

Torres, M. A., West, A. J., Clark, K. E., Paris, G., Bouchez, J., Ponton, C., et al. (2016). The acid and alkalinity budgets of weathering in the Andes–Amazon system: Insights into the erosional control of global biogeochemical cycles. *Earth and Planetary Science Letters*, *450*, 381–391. https://doi.org/10.1016/j.epsl.2016.06.012

van der Meulen, B., Gingerich, P. D., Lourens, L. J., Meijer, N., van Broekhuizen, S., van Ginneken, S., & Abels, H. A. (2020). Carbon isotope and mammal recovery from extreme greenhouse warming at the Paleocene–Eocene boundary in astronomically-calibrated fluvial strata, Bighorn Basin, Wyoming, USA. *Earth and Planetary Science Letters*, *534*, 116044. https://doi.org/10.1016/j.epsl.2019.116044

Wang, C., Adriaens, R., Hong, H., Elsen, J., Vandenberghe, N., Lourens, L. J., et al. (2017). Clay mineralogical constraints on weathering in response to early Eocene hyperthermal events in the Bighorn Basin, Wyoming (Western Interior, USA). *The Geological Society of America Bulletin*, *129*(7–8), 997–1011. https://doi.org/10.1130/b31515.1

Whipple, K. X. (2009). The influence of climate on the tectonic evolution of mountain belts. *Nature Geoscience*, *2*(2), 97–104. https://doi.org/10.1038/ngeo413

White, A. F., & Buss, H. L. (2014). Natural weathering rates of silicate minerals. In *Treatise on Geochemistry* (2nd ed., pp. 115–155). Elsevier.

Wing, S. L., Alroy, J., & Hickey, L. J. (1995). Plant and mammal diversity in the Paleocene to early Eocene of the Bighorn Basin. *Palaeogeography, Palaeoclimatology, Palaeoecology*, *115*(1–4), 117–155. https://doi.org/10.1016/0031-0182(94)00109-1

Wing, S. L., & Currano, E. D. (2013). Plant response to a global greenhouse event 56 million years ago. *American Journal of Botany*, *100*(7), 1234–1254. https://doi.org/10.3732/ajb.1200554

Wing, S. L., & Greenwood, D. R. (1993). Fossils and fossil climate: The case for equable continental interiors in the Eocene. *Philosophical Transactions of the Royal Society of London Series B Biological Sciences*, *341*(1297), 243–252.

Wing, S. L., Harrington, G. J., Smith, F. A., Bloch, J. I., Boyer, D. M., & Freeman, K. H. (2005). Transient floral change and rapid global warming at the Paleocene-Eocene boundary. *Science*, *310*(5750), 993–996. https://doi.org/10.1126/science.1116913

Winnick, M. J., & Maher, K. (2018). Relationships between $CO_2$, thermodynamic limits on silicate weathering, and the strength of the silicate weathering feedback. *Earth and Planetary Science Letters*, *485*, 111–120. https://doi.org/10.1016/j.epsl.2018.01.005

## References From the Supporting Information

Abels, H. A., Kraus, M. J., & Gingerich, P. D. (2013). Precession-scale cyclicity in the fluvial lower Eocene Willwood Formation of the Bighorn Basin, Wyoming (USA). *Sedimentology*, *60*(6), 1467–1483. https://doi.org/10.1111/sed.12039

Aslan, A., & Autin, W. J. (1998). Holocene flood-plain soil formation in the southern lower Mississippi Valley: Implications for interpreting alluvial paleosols. *The Geological Society of America Bulletin*, *110*(4), 433–449. https://doi.org/10.1130/0016-7606(1998)110<0433:hfpsfi>2.3.co;2

Bown, T. M., & Kraus, M. J. (1981). Lower Eocene alluvial paleosols (Willwood Formation, northwest Wyoming, USA) and their significance for paleoecology, paleoclimatology, and basin analysis. *Palaeogeography, Palaeoclimatology, Palaeoecology*, *34*, 1–30. https://doi.org/10.1016/0031-0182(81)90056-0

Bown, T. M., & Kraus, M. J. (1987). Integration of channel and floodplain suites; I, Developmental sequence and lateral relations of alluvial Paleosols. *Journal of Sedimentary Research*, *57*(4), 587–601.

Clyde, W. C., Hamzi, W., Finarelli, J. A., Wing, S. L., Schankler, D., & Chew, A. (2007). Basin-wide magnetostratigraphic framework for the Bighorn Basin, Wyoming. *The Geological Society of America Bulletin*, *119*(7–8), 848–859. https://doi.org/10.1130/b26104.1

Daniels, J. M. (2003). Floodplain aggradation and pedogenesis in a semiarid environment. *Geomorphology*, *56*(3–4), 225–242. https://doi.org/10.1016/s0169-555x(03)00153-3

DeCelles, P. G., Gray, M. B., Ridgway, K. D., Cole, R. B., Pivnik, D. A., Pequera, N., & Srivastava, P. (1991a). Controls on synorogenic alluvial-fan architecture, Beartooth Conglomerate (Palaeocene), Wyoming and Montana. *Sedimentology*, *38*(4), 567–590. https://doi.org/10.1111/j.1365-3091.1991.tb01009.x

DeCelles, P. G., Gray, M. B., Ridgway, K. D., Cole, R. B., Srivastava, P., Pequera, N., & Pivnik, D. A. (1991b). Kinematic history of a foreland uplift from Paleocene synorogenic conglomerate, Beartooth Range, Wyoming and Montana. *The Geological Society of America Bulletin*, *103*(11), 1458–1475. https://doi.org/10.1130/0016-7606(1991)103<1458:khoafu>2.3.co;2

Fan, M., & Carrapa, B. (2014). Late Cretaceous–early Eocene Laramide uplift, exhumation, and basin subsidence in Wyoming: Crustal responses to flat slab subduction. *Tectonics*, *33*(4), 509–529. https://doi.org/10.1002/2012tc003221

Finn, T. M. (2019). *Stratigraphic cross sections of the Niobrara Interval of the Upper Cretaceous Cody Shale in the Bighorn Basin, Wyoming and Montana* (No. 3422). US Geological Survey.

Foreman, B. Z. (2014). Climate-driven generation of a fluvial sheet sand body at the Paleocene–Eocene boundary in north-west Wyoming (USA). *Basin Research*, *26*(2), 225–241. https://doi.org/10.1111/bre.12027

Gingerich, P. D. (2001). Biostratigraphy of the continental Paleocene-Eocene boundary interval on Polecat Bench in the northern Bighorn Basin. Paleocene-Eocene stratigraphy and biotic change in the Bighorn and Clarks Fork basins. *Wyoming*, *33*, 37–71.

Gingerich, P. D. (2010). Mammalian faunal succession through the Paleocene-Eocene Thermal Maximum (PETM) in western North America. *Vertebrata Palasiatica*, *48*, 308–327.

Hajek, E. A., & Wolinsky, M. A. (2012). Simplified process modeling of river avulsion and alluvial architecture: Connecting models and field data. *Sedimentary Geology*, *257*, 1–30. https://doi.org/10.1016/j.sedgeo.2011.09.005

Kraus, M. J. (1980). Genesis of a fluvial sheet sandstone, Willwood Formation, northwest Wyoming. *Early Cenozoic Paleontology and Stratigraphy of the Bighorn Basin, Wyoming. University of Michigan Papers on Paleontology*, *24*, 87–94.

Kraus, M. J., & Aslan, A. (1993). Eocene hydromorphic Paleosols; significance for interpreting ancient floodplain processes. *Journal of Sedimentary Research*, *63*(3), 453–463.

Kraus, M. J., & Hasiotis, S. T. (2006). Significance of different modes of rhizolith preservation to interpreting paleoenvironmental and paleohydrologic settings: Examples from Paleogene paleosols, Bighorn Basin, Wyoming, USA. *Journal of Sedimentary Research*, *76*(4), 633–646. https://doi.org/10.2110/jsr.2006.052

Kraus, M. J., & Middleton, L. T. (1987). Contrasting architecture of two alluvial suites in different structural settings. *Society of Economic Paleontologists and Mineralogists. Recent Developments in Fluvial Sedimentology*, *30*, 253–262. https://doi.org/10.2110/pec.87.39.0253

Li, W., Liu, X. M., & Chadwick, O. A. (2020). Lithium isotope behavior in Hawaiian regoliths: Soil-atmosphere-biosphere exchanges. *Geochimica et Cosmochimica Acta*, *285*, 175–192. https://doi.org/10.1016/j.gca.2020.07.012

Love, J. D., & Christiansen, A. C. (1985). Geologic Map of Wyoming: US Geologic Survey, scale 1: 500,000.

Magna, T., Wiechert, U. H., & Halliday, A. N. (2004). Low-blank isotope ratio measurement of small samples of lithium using multiple-collector ICPMS. *International Journal of Mass Spectrometry*, *239*(1), 67–76. https://doi.org/10.1016/j.ijms.2004.09.008

Neasham, J. W., & Vondra, C. F. (1972). Stratigraphy and petrology of the lower Eocene Willwood Formation, Bighorn Basin, Wyoming. *The Geological Society of America Bulletin*, *83*(7), 2167–2180. https://doi.org/10.1130/0016-7606(1972)83[2167:sapotl]2.0.co;2

Qi, T., Odagiri, T., & Nomura, M. (1997). Extraction of lithium from GSJ rock reference samples and determination of their lithium isotopic compositions. *Analytica Chimica Acta*, *340*(1–3), 221–225. https://doi.org/10.1016/s0003-2670(96)00519-3

Smith, J. J., Hasiotis, S. T., Kraus, M. J., & Woody, D. T. (2008). Relationship of floodplain ichnocoenoses to paleopedology, paleohydrology, and paleoclimate in the Willwood Formation, Wyoming, during the Paleocene–Eocene Thermal Maximum. *Palaios*, *23*(10), 683–699. https://doi.org/10.2110/palo.2007.p07-080r

Thomas, L. E. (1965). Sedimentation and structural development of Big Horn basin. *American Association of Petroleum Geologists Bulletin*, *49*(11), 1867–1877. https://doi.org/10.1306/a6633870-16c0-11d7-8645000102c1865d

Westerhold, T., Röhl, U., Donner, B., & Zachos, J. C. (2018). Global extent of early Eocene hyperthermal events: A new Pacific benthic foraminiferal isotope record from Shatsky Rise (ODP Site 1209). *Paleoceanography and Paleoclimatology*, *33*(6), 626–642. https://doi.org/10.1029/2017pa003306

Whalley, C., & Grant, A. (1994). Assessment of the phase selectivity of the European Community Bureau of Reference (BCR) sequential extraction procedure for metals in sediment. *Analytica Chimica Acta*, *291*(3), 287–295. https://doi.org/10.1016/0003-2670(94)80024-3

Zielhofer, C., Espejo, J. M. R., Granados, M. À. N., & Faust, D. (2009). Durations of soil formation and soil development indices in a Holocene Mediterranean floodplain. *Quaternary International*, *209*(1–2), 44–65. https://doi.org/10.1016/j.quaint.2009.02.023